RSC Advances




ROYAL SOCIETY OF CHEMISTRY

www.rsc.org/advances

RSC Advances

RSCPublishing

ARTICLE

# A Model for the Impact of the Nanostructure Size on its Gas Sensing Properties

Cite this: DOI: 10.1039/x0xx00000x

Mohammad R. Alenezi,[a] T. H. Alzanki,[a] A. M. Almeshal,[a] A. S. Alshammari,[b] M. J. Beliatis,[c] S. J. Henley [d] and S. R. P. Silva [d]

Received 00th January 2012,
Accepted 00th January 2012

DOI: 10.1039/x0xx00000x

www.rsc.org/

The size of a metal oxide nanostructure plays a key role in its performance as a gas sensor. ZnO nanostructures with different morphologies including nanowires at different diameters and nanodisks at different thicknesses were synthesized hydrothermally. Gas sensors based on individual nanostructures with different sizes were fabricated and their sensing properties were compared and investigated. Nanowires with smaller diameter size and higher surface to volume ratio showed enhanced gas sensing performance. Also, as the nanodisk thickness gets closer to the thickness of the ZnO depletion layer, the sensitivity increases significantly due to the semi complete depletion of the nanostructure. Our results were explained using a modified general formula for ZnO ethanol sensor. The formula was established based on the chemical reaction between ethanol molecules and oxygen ions and considering the effect of the surface to volume ratio as well as the depletion region of the nanostructure. This work can be simply generalized for other metal oxides to enhance their performance as gas sensors.



## Introduction

Air pollution is significantly responsible for different health problems including respiratory infections, heart disease, COPD, stroke and lung cancer.[1] Children living in developing countries have the highest death rate in population caused by indoor and outdoor air pollution.[2] Air pollution worries many countries and the need for clean environment is vital for human health. Based on the World Health Organization reports, the Indian nation faces the greatest challenge and has the highest death rate because of air pollution.[2] In the European Union, air pollution is said to lower the expected life time by 9 months.[2] Therefore, gas sensors that can detect explosives and toxic gases are very important. Also, the performance of the available gas sensors must be improved in term of sensitivity, selectivity, stability, and speed of response to face these great challenges.

Gas sensors based on metal oxides have been broadly investigated for different reasons including ease of production and low cost. Nevertheless, the gas sensing properties of these sensors depend greatly on their size, morphology and structure of the sensing materials. That is why it is very challenging for gas sensors based on bulk materials to attain high sensing performance. On the other hand, nanostructured metal oxides provide a sensible alternative to achieve the required performance. Nanostructured gas sensors based on different metal oxides have been widely studied in recent years.[3–6] Among them, ZnO has received the greatest deal of attention due to the significant progress and development in the controlled synthesis of many of its nanostructures.[7–12] In our previous reports, the synthesis techniques as well as the sensing properties of sensors based on ZnO nanostructures with different morphologies including nanowires (NWs), nanodisks, nanobrushes, hierarchical nanodisks, nanoleaves, and nanoflakes were presented.[10–17] Moreover, the role of the exposed polar facets of the nanostructure on its performance as a gas sensor was investigated in another report.[18] Even though, there are reports on nanostructured metal oxide gas sensors, a deeper understanding of the impact of the nanostructure size on its performance as a gas sensor is still needed.

Our studies as well as many in the literature concluded that the morphology and size of nanostructure used in the sensor have a strong impact on its response characteristics. Different models have been presented trying to explain sensor response characteristics. A contact controlled model[19] and surface-depletion controlled model[20] were proposed to explain the enhanced ethanol gas sensing properties of nanostructures. Similarly, Chen et al.[21] have used space-charge model to explain ultrahigh sensitivity to ethanol of ZnO flowers consisting from 15 nm thick nanowires. The density functional theory (DFT) was also applied to better understand the sensing mechanism of ZnO nanostructures.[22] The outcome of this study was an exponential formula of ZnO sensor response. Based on

that, Hongsith and co-workers tried to generalize a formula of ZnO gas sensors based on ethanol adsorption mechanism.[23]
In this report, a general formula for ZnO ethanol sensor is established by considering ethanol molecules reacting with oxygen ions and taking the surface depletion layer in account. The developed general formula is then used to explain the enhancement in sensitivity resulting from increased surface-to-volume ratio and surface depletion layer for one-dimensional (1-D) NWs and two-dimensional (2-D) nanodisks. This work can be simply generalized for other metal oxides.

## Gas Sensing

The key concept behind the working principle of gas sensors based on metal oxide semiconductors is the observed impact of the interaction of gas molecules with exposed surfaces of the metal oxide, which is a process related to the chemisorbed oxygen on the surface. At low temperatures, only molecular oxygen is adsorbed on the semiconductor surface holding electrons from the conduction band. However, at higher temperatures 100-450 °C both ionized molecular ($O_2^-$) and atomic ($O^-$, $O^{2-}$) oxygen forms can exist on the surface of the semiconductor.[24]
To explain the interaction between oxygen ions and gas molecules, the general model presented by Hongsith and co-workers of ethanol gas on the surface of an n-type ZnO is used.[23] When ethanol molecules interact with oxygen ions on the ZnO surface, electrons are liberated and sent back to the conduction band as represented in the following reactions in Eqs. (1) and (2) for $O^-$ and $O^{2-}$, respectively.

$$CH_3CH_2OH + O^-_{ads} \xrightarrow{k_{Eth}} C_2H_4O + H_2O + 1e^- \quad (1)$$

$$CH_3CH_2OH + O^{2-}_{ads} \xrightarrow{k_{Eth}} C_2H_4O + H_2O + 2e^- \quad (2)$$

Consequently, the rate equations for the electron density can be produced as follow:

$$\frac{dn}{dt} = k_{Eth}(T)[O^-_{ads}]^1[CH_3CH_2OH]^1 \quad (3)$$

$$\frac{dn}{dt} = k_{Eth}(T)\left[O^{2-}_{ads}\right]^{½}[CH_3CH_2OH]^{½} \quad (4)$$

$$\frac{dn}{dt} = k_{Eth}(T)\left[O^{ion}_{ads}\right]^b[CH_3CH_2OH]^b \quad (5)$$

In eq. (5), (*n*) is the electron density, (*b*) can take the value of 1 for singly charged oxygen and 0.5 for doubly charged oxygen, and $k_{Eth}(T)$ represents the reaction rate constant.
By solving the integration of eq (5), *n* can presented as follow:

$$n = k_{Eth}(T)\left[O^{ion}_{ads}\right]^b[CH_3CH_2OH]^b t + n_0 \quad (6)$$

In this case the electron concentration in air is ($n_0$). It is assumed that both carrier concentrations *n* and $n_0$ under ethanol and air are independent of time at equilibrium.

Therefore, Eq. (6) can become

$$n = \Gamma_t k_{Eth}(T)\left[O^{ion}_{ads}\right]^b[CH_3CH_2OH]^b t + n_0 \quad (7)$$

where $\Gamma_t$ is a time constant and the carrier-concentration $n = \alpha/R$, where R is the resistance and α is a proportionality factor. Substituting it in Eq. (7) gives the following eq:

$$\frac{1}{R_g} = \frac{\Gamma_t k_{Eth}(T)\left[O^{ion}_{ads}\right]^b[CH_3CH_2OH]^b t}{\alpha} + \frac{1}{R_a} \quad (8)$$

The sensor sensitivity, $S_g = R_a/R_g$ where $R_a$ is the sensor resistance in air, and $R_g$ is the sensor resistance under ethanol gas. Thus,

$$S_g = \frac{R_a}{R_g} = \frac{\Gamma_t k_{Eth}(T)\left[O^{ion}_{ads}\right]^b[CH_3CH_2OH]^b t}{n_0} + 1 \quad (9)$$

Eq (9) can be rewritten in a compressed form relating the sensitivity to ethanol concentration ($C_g$) as follow:[23]

$$S_g = aC_g^b + 1 \quad (10)$$

where a is a parameter and eq (10) can be represented as:

$$\log(S_g - 1) = \log a + b\log C_g \quad (11)$$

From this relation it can be realized that log ($S_g$ −1) is linearly related to log $C_g$ with a slope of *b* value.
As stated before, the increased surface area is the key factor behind the enhancement observed when nanomaterials are used as sensing materials. In fact, the density of adsorbed oxygen ions is predominantly controlled by the surface-to-volume ratio of the nanostructure. Therefore, it should be considered in the formula of the sensitivity. The following equation shows the dependence of the density of adsorbed oxygen ions on the surface-to-volume ratio of the structure.

$$\left[O^{ion}_{ads}\right] = \frac{\sigma_0(S/V)V_m}{V_s} \quad (12)$$

where $\sigma_0$ is the oxygen ion density, (*S/V*) is a surface area ratio per volume of material ($V_m$), and $V_s$ is the volume of the system. The substitution of Eq. (12) onto Eq. (9) gives the sensitivity as follow

$$S_{(S/V)} = \frac{R_a}{R_g} = \frac{\Gamma_t k_{Eth}(T)\left[\frac{\sigma_0(S/V)V_m}{V_s}\right]^b}{n_0} C_g^b + 1 \quad (13)$$

The width of the surface charge region (*W*) is represented below.

$$W = L_d\,(eV_s/kT)^{1/2} \quad (14)$$

where $L_d$ is the Debye length and $V_s$ is band bending induced by the adsorbates. The Debye length is used to scale the depletion region of the NW. At a distance that is equal to several Debye



 

lengths from the surface of the NW, the carriers' density is equal to the bulk value. Therefore, for large enough NWs (> $2L_d$) bulk characteristics are assumed. The following equation is used to evaluate the Debye length.

$$L_d = \left[\frac{\varepsilon k_B T}{q^2 n}\right]^{1/2} \quad (15)$$

where ε is the relative dielectric permittivity of the nanostructure and $n$ is the charge-carrier density. It is clear that as the $L_d$ increases with temperature and decays with growing density of donor defects.

## Experimental

The preparation of ZnO NWs and nanodisks is reported before.[11] Briefly, ZnO NWs were produced through a seed layer assisted hydrothermal synthesis method using a mixture solution of zinc nitrate, hexamethylenetetramine (HMTA), Ammonium hydroxide and polyethylenimine (PEI) (end-capped, molecular weight 800 g/mol LS, Aldrich). On the other hand, ZnO nanodisks were produced hydrothermally using a mixture solution of zinc sulphate and HMTA.

The morphology and crystal structure of as-prepared products were observed using Philips XL-20 scanning electron microscope at 10 kV. Photoluminescence (PL) spectroscopy was performed at room temperature using a Cary Eclipse spectrometer with an excitation wavelength of 325 nm. The surface composition of the ZnO samples were determined using PHI QUANTUM 2000 photoelectron spectrometer (XPS) using a monochromatic magnesium X-ray source. The binding energies were calibrated with respect to the signal for adventitious carbon (binding energy of 284.6 eV).

Three NW gas sensors were fabricated based on individual NWs with diameters of 400, 150, and 85 nm on SiO2/Si substrates with pre-patterned gold electrodes. The spacing between the electrodes was 5 µm. Moreover, three nanodisk gas sensors were also fabricated based on individual nanodisks with thicknesses of 150, 100, and 50 nm on $SiO_2$/Si substrates with pre-patterned gold electrodes. The spacing between the electrodes was 2.5 µm. Before measurement, sensors fabricated were further aged at 200 °C for 2 days to improve the stability before testing. The gas sensing properties were measured using a home-made gas sensing chamber attached to a Keithley 4200 semiconductor analyzer.

The sensor response, Sg, is defined as $Sg = I_g/I_a$, where Ig is the sensor current value in the tested gas environment and Ia is the current value in air. The measurements were done under fixed bias. The response time, $t_r$, is defined as the time required for the current to reach 90% of the equilibrium value after injecting the gas, and the recovery time, $t_d$, is defined as the time necessary for the sensor to return to 10% above the original current value in air after releasing the gas from the test chamber.

## Results and discussion

First, the impact of the diameter size of the ZnO NW on its performance as gas sensor is investigated by studying and comparing gas sensors fabricated based on NWs with different diameters (400, 150, and 85 nm). The operating temperature is an important parameter that affects the performance of ZnO gas sensors greatly. All fabricated ZnO sensors have been tested at a range of temperatures in order to find the optimum working temperature for Ethanol detection. We observed that the sensitivity toward ethanol of all ZnO NW sensors increases as the operating temperature increases up to 300 °C and decreases with any further increase in the operating temperature. The reason behind this phenomenon is that metal-oxide sensors must get enough thermal energy to activate. At low working temperatures, ZnO NWs are not chemically active and subsequently cannot sense ethanol. Conversely, when the working temperature is relatively high, there would be a significant increase in activation which forces ethanol molecules adsorbed on the ZnO surface to leave the surface without exchanging charges. Meaning that, ZnO sensors in this case are also less sensitive.[15]

Figure 1 shows an SEM image of a sensor based on a 400 nm ZnO NW ($ZNW_{400}$) as well as its ethanol gas sensing characteristics at 300 °C for different concentration levels. For ethanol at levels of 100, 300 and 500 ppm, the $ZNW_{400}$ sensor responses are 4.3, 9, and 13.4, respectively (figure 1(a)). Figure 1(c) show plots of log ($S_g$ −1) versus log $C_g$ for the $ZNW_{400}$ sensor where a linear relationship as described by Eq. (11) is observed. The value of $b$ of this sensor is 0.560. This value suggests that the dominant adsorbed oxygen species at the surface of the $ZNW_{400}$ sensor are $O^{2-}$ ions. [18,24]

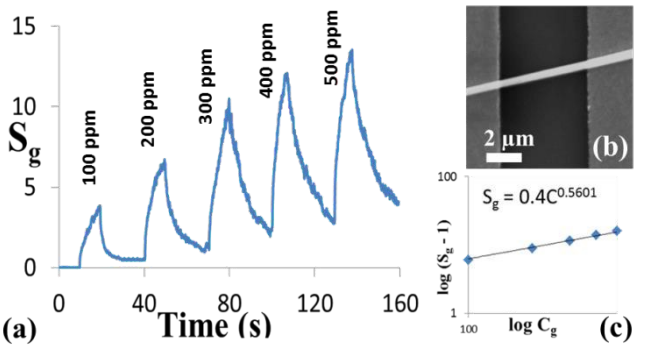


**Figure 1** (a) Ethanol gas sensing characteristics, (b) an SEM image and (c) log (Sg - 1) vs. log Cg plot of the $ZNW_{400}$ gas sensor.

Figure 2 shows an SEM image of a sensor based on a 150 nm ZnO NW ($ZNW_{150}$) as well as its ethanol gas sensing characteristics at 300 °C for different concentration levels. For ethanol at levels of 100, 300 and 500 ppm, the $ZNW_{150}$ sensor responses are 7, 15, and 22.5, respectively (figure 2(a)). Figure 2(c) show plots of log ($S_g$ −1) versus log $C_g$ for the $ZNW_{150}$ sensor where a linear relationship as described by Eq. (11) is observed. The value of $b$ of this sensor is 0.5665 which suggests that the $O^{2-}$ ions are the dominant adsorbed oxygen species at the surface of the $ZNW_{150}$.[18,24]

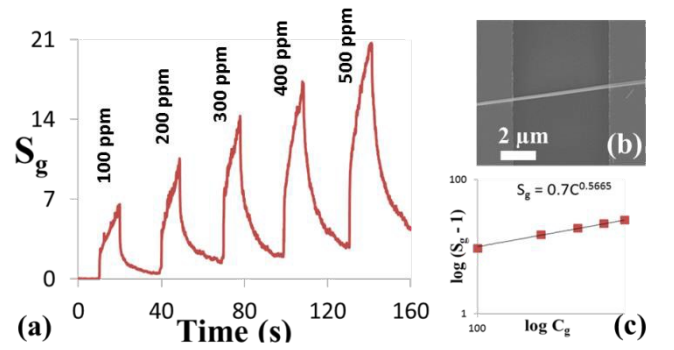


**Figure 2** (a) Ethanol gas sensing characteristics, (b) an SEM image and (c) log (Sg - 1) vs. log Cg plot of the ZNW150 gas sensor.

Figure 3 shows an SEM image of a sensor based on an 85 nm ZnO NW ($ZNW_{85}$) as well as its ethanol gas sensing characteristics at 300 ˚C for different concentration levels. For ethanol at levels of 100, 300 and 500 ppm, the $ZNW_{150}$ sensor responses are 11.2, 21.4, and 33, respectively (figure 3(a)). Figure 3(c) show plots of log ($S_g$ −1) versus log $C_g$ for the $ZNW_{85}$ sensor where a linear relationship as described by Eq. (11) is observed. The value of *b* of this sensor is 0.5722 suggesting $O^{2-}$ ions species on the surface of the $ZNW_{85}$ sensor.[18,24]

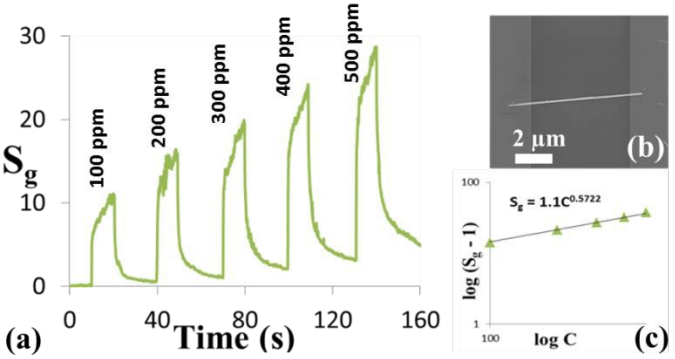


**Figure 3** (a) Ethanol gas sensing characteristics, (b) an SEM image and (c) log ($S_g$ - 1) vs. log $C_g$ plot of the $ZNW_{85}$ gas sensor.

The diameters of the $ZNW_{400}$, $ZNW_{150}$, and $ZNW_{85}$ are fairly greater than the Debye length. Therefore, in this case the impact of the depletion region is limited and the surface-to-volume ratio (S/V) of these nanostructures is expected to be the predominant factor in the gas sensing performance represented in Eq. (13).[23] The dependence of sensitivity on the diameter of the NW can be clarified by calculating the surface-to-volume ratio and applying them in Eq. (16) for the sensor sensitivity ratio.[18]

$$\frac{S_g(ZNW_B)-1}{S_g(ZNW_A)-1} = \left[\frac{(S/V)_B}{(S/V)_A}\right]^b \approx \left[\frac{D_A}{D_B}\right]^b \qquad (16)$$

Table 1 presents the calculated sensitivity ratios of each two sensors at different ethanol concentrations of 100, 300, and 500 as well as their corresponding experimental results. Compared with their corresponding surface-to-volume ratios presented in the last row, a good agreement is noticed. Hence, it is concluded that the increase in the surface-to-volume ratio enhances the sensitivity. Furthermore, comparing the sensor response characteristics of the three tested sensors $ZNW_{400}$, $ZNW_{150}$, and $ZNW_{85}$ depicted in figures 1(b), 2(b) and 3(b), respectively, it is clear that increasing the surface-to-volume ratio of the NW also enhances the speed of response and recovery.

**Table 1** The sensitivity ratios of the NW sensors compared to their surface-to-volume ratios.

| Sensitivity Ratio / Ethanol Concentration | $\frac{S_g(ZNW_{85})-1}{S_g(ZNW_{400})-1}$ | $\frac{S_g(ZNW_{85})-1}{S_g(ZNW_{150})-1}$ | $\frac{S_g(ZNW_{150})-1}{S_g(ZNW_{400})-1}$ |
|---|---|---|---|
| 100 ppm | 2.48 | 1.36 | 1.8 |
| 300 ppm | 2.55 | 1.45 | 1.73 |
| 500 ppm | 2.42 | 1.39 | 1.69 |
| $\left[\frac{D_A}{D_B}\right]^{0.5}$ | 2.17 | 1.33 | 1.633 |

In the rest of this section, the impact of the thickness of the ZnO nanodisk on its performance as gas sensor is investigated by comparing sensors fabricated based on nanodisks with different thicknesses. Figures 4(a)-(c) show SEM images of ZnO nanostructured gas sensors based on individual ZnO nanodisks with thicknesses of 150, 100, and 50 nm, respectively. Plots of the sensitivity of the three ZnO nanodisk gas sensors ($ZND_{150}$, $ZND_{100}$, and $ZND_{50}$) versus ethanol gas concentrations under the optimum operating temperature of 350 ˚C are shown in figure 4(d).

For ethanol at concentration levels of 100, 300 and 500 ppm, the $ZND_{150}$ sensor responses are 12, 21, and 28, respectively. The responses of the $ZND_{100}$ to the same levels of ethanol concentrations are 19, 33, and 45, respectively. The third gas sensor based on the thinnest $ZND_{50}$ showed the highest gas responses of 166, 298, and 403 to ethanol concentrations of 100, 300, and 500, respectively.

Figure 4(e) show plots of log ($S_g$ −1) versus log $C_g$ for the three devices where linear relationships are observed. The value of *b* of the $ZND_{150}$, $ZND_{100}$, and $ZND_{50}$ sensors are 0.523, 0.519, and 0.538, respectively. These values suggest that the dominant adsorbed oxygen species at the surface of the three ZND sensors are $O^{2-}$ ions. At constant temperatures, the existence of these ions on the nanodisk surface builds a depletion layer by seizing electrons from the conduction band dropping the conductivity of the ZnO nanodisk.[18]

Applying the same model used in the NWs case which considering only the surface-to-volume ratio of the nanostructure, the sensitivity ratio of the nanodisk sensors with

| Ethanol Concentration \ Sensitivity Ratio | $\frac{S_g(ZNW_{100})-1}{S_g(ZNW_{150})-1}$ | $\frac{S_g(ZNW_{50})-1}{S_g(ZNW_{100})-1}$ | $\frac{S_g(ZND_{50})-1}{S_g(ZND_{150})-1}$ |
|---|---|---|---|
| 100 ppm | 1.70 | 8.70 | 13.90 |
| 300 ppm | 1.65 | 9.06 | 14.20 |
| 500 ppm | 1.60 | 8.97 | 14.40 |
| $\left[\frac{Th_B}{Th_A}\right]^{0.5}$ | 1.22 | 1.41 | 1.73 |
| $\left[\frac{Th_B}{Th_A}\right]^{0.5}\left(\frac{Th_A}{Th_A-2L_d}\right)\left(\frac{Th_B-2L_d}{Th_B}\right)$ | 1.57 | 9.55 | 15.01 |

different thicknesses, $Th_{150}$, $Th_{100}$, and $Th_{50}$ can be represented as follow:

$$\frac{S_g(Th_A)-1}{S_g(Th_B)-1}=\left[\frac{(S/V)_A}{(S/V)_B}\right]^b=\left[\frac{Th_B}{Th_A}\right]^{0.5} \quad (17)$$

The sensitivity ratios that are calculated using equation (17) and those based on our experimental results are shown in table 2. On one hand, the difference between the calculated and measured sensitivity ratios of $ZND_{150}$ and $ZND_{100}$ is around 35 %. On the other hand, the differences between the calculated and measured sensitivity ratios when comparing the sensitivity of $ZND_{50}$ with those of $ZND_{100}$ and $ZND_{150}$ are 532 % and 719 %, respectively. A significant variation in the differences in the three cases is observed. The calculations that are obtained using surface-to-volume ratio model are only acceptable for the sensitivity ratio between $ZND_{150}$ and $ZND_{100}$. The calculations for the other two cases involving $ZND_{50}$ are not satisfactory and the applied model must be improved. The calculated Debye length of ZnO ($L_d$) is 23 nm which is comparable to the values reported in the literature about 30 nm.[25,26] Since the value of $2L_d$ = 46 nm, it is suspected that the reason behind the observed significant variation is that the thickness of the $ZND_{50}$ is comparable to twice the Debye length. Hence, in the following section the model is developed to consider the influence of the surface-to-volume ratio as well as the effect of the depletion region.

As discussed earlier, under ethanol environment its gas molecules react with oxygen ions on the ZnO nanodisk surface resulting in more free electrons. This lowers the width of the depletion layer and enhances the conductivity of the ZnO nanodisk subsequently. Therefore, the density of carriers has a significant impact on the thickness of the conductivity channel, and is represented using ($L_d$) as follow:

$$\bar{n}=n_0\frac{(Th-2L_d)}{Th} \quad (18)$$

where $n_0$ is the density of carriers concentration of intrinsic material, $\bar{n}$ represents the density of carriers in the depletion region, and $Th$ is thickness of the ZnO nanodisk. Hence, we can represent the impact of the surface-to-volume ratio along with that of the depletion region on the response of the ZnO nanodisk sensor as follow:

$$S_{(L_d)}=\frac{R_a}{R_g}=\left(\frac{\Gamma_t k_{Eth}(T)\left[\frac{\sigma_0(S/V)V_m}{V_S}\right]^b}{n_0}\right)C_g^b\left(\frac{Th}{Th-2L_d}\right)+1 \quad (19)$$

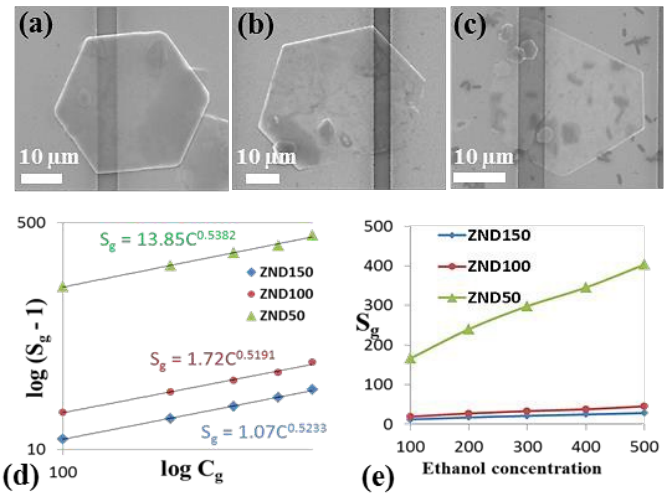


**Figure 4** SEM images of the (a) $ZND_{150}$, (b) $ZND_{100}$, and (c) $ZND_{50}$; (d) Sensitivity versus ethanol gas concentration, and (e) log ($S_g$ -1) vs. log $C_g$ plot of the ZND gas sensors.

The sensitivity ratio considering the influence of the surface-to-volume ratio as well as the effect of the depletion region between two sensors that are based on two nanodisks with different thicknesses is represented as follow:

$$\frac{S_g(Th_A)-1}{S_g(Th_B)-1}=\left[\frac{(S/V)_A}{(S/V)_B}\right]^b\left(\frac{Th_A}{Th_A-2L_d}\right)\left(\frac{Th_B-2L_d}{Th_B}\right)=\left[\frac{Th_B}{Th_A}\right]^{0.5}\left(\frac{Th_A}{Th_A-2L_d}\right)\left(\frac{Th_B-2L_d}{Th_B}\right) \quad (20)$$

The calculated sensitivity ratios of the three nanodisk sensors as well as the experimental results are shown in table 2. It is evident that after considering the effect of the depletion region the calculated results are in a good agreement with the experimental measurements in all cases. The difference between the calculated and measured sensitivity ratios between

$ZND_{150}$ and $ZND_{100}$ is only 5 % now. Furthermore, the differences between the calculated and measured sensitivity ratios when comparing the sensitivity of $ZND_{50}$ with those of $ZND_{100}$ and $ZND_{150}$ are 6.7 % and 5.6 %, respectively. The $ZND_{50}$ sensor with a thickness value that is comparable to twice the Debye length value ($2L_d$) showed an outstanding performance. These results suggest that the sensitivity enhancement of the ZnO nanodisk sensor is prominent when the thickness of the nanodisk is close to 50 nm.

Figure 5 presents the $ZND_{50}$ sensor response to ethanol concentration levels from 1 to 500 ppm. The $ZND_{50}$ sensor demonstrates impressive response characteristics in comparison with the rest of the tested ZnO nanostructures in this study as well as those reported in the literature.[27-30] The response time and recovery time of the $ZND_{50}$ sensor to 5 ppm ethanol are about 10 and 13 s, respectively. With the increase in ethanol concentration, the response time decreases gradually. The response times are calculated to be approximately 8 s for 20 ppm acetone and 4 s for 100 ppm. The decrease in response time can be explained by the variation of the saturation time (the time required for complete coverage of the sensor surface by the ethanol molecules) and the mean residence period of acetone molecules on the $ZND_{50}$ surface. When the concentration of ethanol is low, the reaction between ethanol molecules and oxygen species occurs in a relatively long period of time which slows the response of the sensor. On the other hand, when ethanol concentration is at higher level, the time needed for the reaction is decreased causing the response time to be shorter.

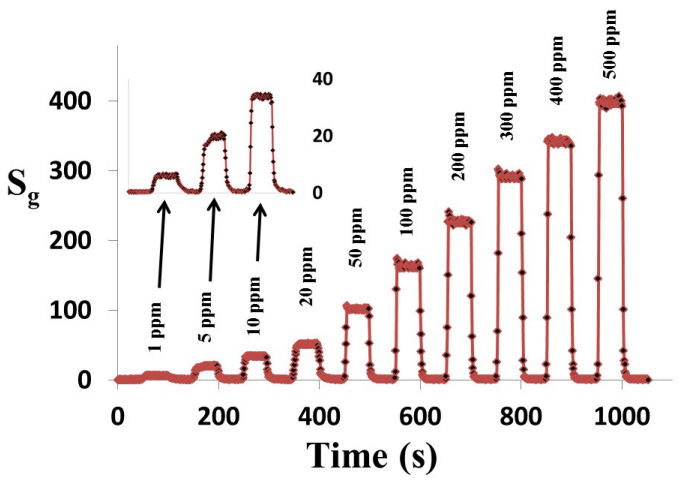


**Figure 5** The $ZND_{50}$ sensor response *vs.* time curve to ethanol concentration levels from 1 to 500 ppm.

ZnO NW and ZND nanostructures obviously have different morphologies and exposed facets, which allow them to have different physical and chemical properties.[15] The NW is a 1D structure with nonpolar exposed facet as can be seen from the NW SEM images shown in figures 1-3. On the other hand, the ZND is 2D structure with polar exposed facets as shown in figure 4. Polar exposed facets can be more active and have a higher ability to absorb oxygen as we found from the following PL and XPS analysis, which affect gas sensing properties greatly.[18]

XPS analysis was performed to investigate surface structure of the two ZnO nanostructures. Figure 6a shows the Zn 2p XPS peaks of ZnO NWs and ZNDs. The two Zn 2p XPS peaks are similar for their position and distribution. On the contrary, we noted a difference in their corresponding O 1s XPS peaks. In both peaks are asymmetric and show a visible shoulder. As presented in figure 6b-c both O 1s XPS peaks can be decomposed into three Gaussian components centered at ~ 530.1 eV ($O_L$), 531.5 eV ($O_V$), and 532.5 eV ($O_C$). The $O_L$ element of O 1s spectrum is ascribed to $O^{2-}$ ions on wurtzite structure of hexagonal $Zn^{2+}$ ion array, surrounded by Zn atoms with their full complement of nearest-neighbour $O^{2-}$ ions. The binding energy element $O_V$ is due to $O^{2-}$ ions in oxygen-deficient regions within the matrix of ZnO. Finally, the $O_C$ element is ascribed to chemisorbed and dissociated oxygen species.[15] Hence, we can use the $O_C$ intensity of the different ZnO nanostructures to measure the oxygen-chemisorbed ability of their different exposed facets. The percentages of the $O_C$ element in the two nanostructures are approximately 3% (ZNWs) and 15% (ZNDs). This means that ZNDs with polar exposed facets may absorb more oxygen species than ZnO NWs with nonpolar exposed facets. XPS analysis also suggests that nanostructures with polar exposed facets like ZNDs have better gas sensing properties than nanostructures with nonpolar exposed facets like NWs.

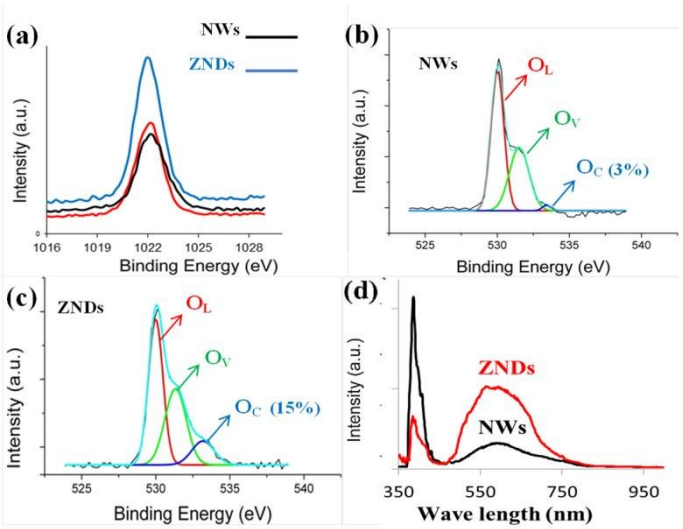


**Figure 6** (a) Zn 2p XPS spectra peaks of ZNWs and ZNDs, (b) O 1s XPS spectra of ZNDs, (c) O 1s XPS spectra of ZnO NWs, and (d) Room temperature PL spectra of ZnO NWs and ZNDs.

Figure 6d shows the PL spectra of the ZnO NWs and ZNDs. From the plots, we can see two bands for each ZnO nanostructure. The first band is a luminescence band centered at 386 nm and the second is a broadband in the region of 450-850 nm. The intensity of the broad luminescence band for the ZNDs is obviously greater than that of the NWs. While the peak centered at 386 nm of ZNWs is higher in intensity.[15,18] This

later peak centered at 386 nm (3.22 eV) is usually ascribed to the near band-edge emission of ZnO (3.37 eV) and the free excitons recombination. Conversely, the broad band in the visible light region is considered an indication of the surface oxygen vacancies. Therefore, this analysis shows that ZND has more chemisorbed oxygen on its surface than the NWs, which means that ZND sensor is more sensitive than the NW sensor.

This difference in the abilities of ZnO NWs and ZNDs to absorb oxygen species may explain why each nanostructure has a specific optimum operating temperature (300 ˚C for the ZnO NWs and 350 ˚C for ZNDs). When the operating temperature is low, ZnO sensors show low conductivity, which increases as the operating temperature increase because of the increase in electron density by thermal excitation. With further increase in operating temperature (around 175 °C), the conductivity increases due to oxygen adsorptions on the nanostructure surface. The oxygen chemisorption process at this stage decreases the density of free electrons and challenge the thermal excitation of electrons. This challenge of the two conflicting processes carry on to the complete coverage of nanostructure surface with chemisorbed oxygen species and ZnO sensors demonstrate the maximum sensitivity. No more oxygen can be chemosorbed after this stage and any increase in the operating temperature will only excite electrons thermally and cuase the sensitivity to decrease. Hence, the optimum operating temperature of ZND sensor is greater than that of the NW sensor due to the higher ability of ZND to absorb oxygen species.[15,18]

Furthermore, the ZND gas sensor is tested at the operating temperature of 350 ˚C under a range of reducing gases including methanol, ethanol, acetone, toluene, ammonia, and carbon monoxide. All gases were injected at the concentration level of 100 ppm. The sensitivity values to the tested gases are demonstrated in figure 7. The sensitivity of the ZND sensor toward ammonia and carbon monoxide was low, while it was very high toward ethanol, methanol, and acetone. This variation in sensitivity toward different gases may originate from the effect of operating temperature. Different gases may have different optimum operating temperatures.

## Conclusions

In conclusion, ZnO nanostructures with different morphologies including nanowires at different diameters and nanodisks at different thicknesses were synthesized through low temperature hydrothermal method. Gas sensors based on individual nanostructures with different sizes were fabricated and their performances were compared and investigated. NWs with smaller diameters and higher surface to volume ratios demonstrated improved sensitivity toward ethanol and faster response and recovery characteristics. Moreover, gas sensors fabricated based on nanodisks with thicknesses closer to the thickness of ZnO depletion layer, showed significant increase in sensitivity. This is attributed to the semi complete depletion of the nanodisk. These results were explained based on a general formula for ZnO ethanol sensor that is established by considering a chemical reaction between ethanol molecule and oxygen ions. This work can be generalized for other metal oxides to enhance their performance as gas sensors.

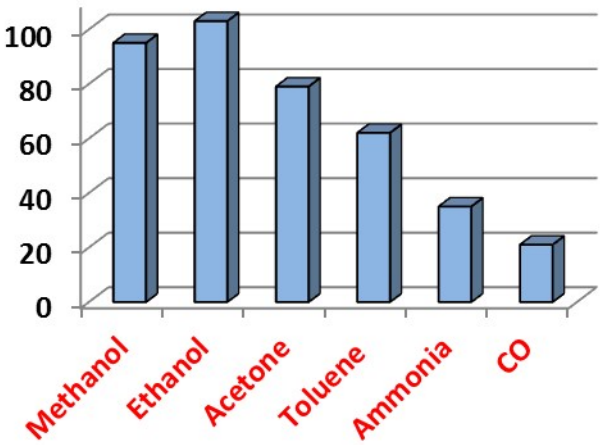


Figure 7 Responses of the ZND gas sensor to 50 ppm of various gases operated at 350 °C.

## Acknowledgements

Mohammad R. Alenezi thanks the Public Authority of Applied Education and Training (PAAET) and the Government of the State of Kuwait for their financial support.

## Notes and references

[a] College of Technological Studies, Public Authority for Applied Education and Training, P.O. Box 42325 Shuwaikh, Kuwait. Email: mr.alenezi@paaet.edu.kw
[b] Department of Physics, College of Science, University of Hail, P.O. Box 2440, Hail, KSA.
[c] Department of Energy Conversion and Storage, Technical University of Denmark, Frederiksborgvej 399, 4000 Roskilde, Denmark.
[d] Nanoelectronics Center, Advanced Technology Institute, University of Surrey, Guildford, GU2 7XH, UK.

1. Air quality and health. WHO. Retrieved 26 Nov 2011.
2. 7 million premature deaths annually linked to air pollution. WHO. Retrieved 25 Mar 2014.
3. Lin Mei, Yuejiao Chen, Jianmin Ma, Gas Sensing of $SnO_2$ Nanocrystals Revisited: Developing Ultra-Sensitive Sensors for Detecting the $H_2S$ Leakage of Biogas. SCIENTIFIC REPORTS 2014, 4, 6028/1−6028/8.
4. Zhiwen Chen, Minghong Wu, Chan-Hung Shek, C. M. Lawrence Wu and Joseph K. L. Lai, Multifunctional tin dioxide materials: advances in preparation strategies, microstructure, and performance. Chem. Commun., 2015, 51, 1175-1184.
5. S. T. Navale, D. K. Bandgar, M. A. Chougule and V. B. Patil, Facile method of preparation of PbS films for $NO_2$ detection. RSC Adv., 2015, 5, 6518-6527.
6. Lichan Chen, Bo Wu, Longhua Guo, Ruiwen Tey, Youju Huang and Dong-Hwan Kim, A single-nanoparticle $NO_2$ gas sensor

constructed using active molecular plasmonics. Chem. Commun., 2015, 51, 1326-1329.
7. Z. Wang, J. Gong, Y. Su, Y. Jiang, S. Yang, Six-Fold-Symmetrical Hierarchical ZnO Nanostructure Arrays: Synthesis, Characterization, and Field Emission Properties. Crystal Growth & Design, 2010, 10, 2455–2459.
8. M. Palumbo, T. Lutz, C. E. Giusca, H. Shiozawa, V. Stolojan, D. C. Cox, R. M. Wilson, S. J. Henley, and S. R. P. Silva, From Stems (and Stars) to Roses: Shape-Controlled Synthesis of Zinc Oxide Crystals. Cryst. Growth Des. 2009, 9, 3432-3437.
9. K. D. G. I. Jayawardena, C. Opoku, J. Fryar, S. R. P. Silva, S. J. Henley, Excimer laser accelerated hydrothermal synthesis of ZnO nanocrystals & their electrical properties. Applied Surface Science. 2010, 257, 5274-5277.
10. M. McCune, W. Zhang, Y. Deng, High Efficiency Dye-Sensitized Solar Cells Based on Three-Dimensional Multilayered ZnO Nanowire Arrays with ``Caterpillar-like" Structure. Nano Lett., 2012, 12, 3656–3662.
11. Mohammad R. Alenezi, Simon J. Henley, Neil G. Emerson, and S. R. P. Silva. From 1D and 2D ZnO nanostructures to 3D hierarchical structures with enhanced gas sensing properties. Nanoscale, 2014, 6, 235−247.
12. Michail J. Beliatis, Keyur K. Gandhi, Lynn J. Rozanski, Rhys Rhodes, Liam McCafferty, Mohammad R. Alenezi, Abdullah S. Alshammari, Christopher A. Mills, K. D. G. Imalka Jayawardena, Simon J. Henley, and S. Ravi P. Silva. Hybrid Graphene-Metal Oxide Solution Processed Electron Transport Layers for Large Area High-Performance Organic Photovoltaics. Advanced Materials, 2014, 26, 2078–2083.
13. Mohammad R. Alenezi, Abdullah S. Alshammari, Peter D. Jarowski, Talal H. Alzanki, Simon J. Henley, and S. R. P. Silva. ZnO nanodisk UV detectors with printed electrodes. Langmuir, 2014, 30, 3913–3921.
14. Mohammad R. Alenezi, Talal H. Alzanki, Abdullah M. Almeshal. Nanowire Array Based UV Detectors. International Journal of Science and Research, 2014, 7, 588–591.
15. Mohammad R. Alenezi, T. H. Alzanki, A. M. Almeshal, A. S. Alshammari, Simon J. Henley, and S. R. P. Silva. Hierarchically Designed ZnO Nanostructures Based High Performance Gas Sensors. RSC Adv., 2014, 4, 49521–49528.
16. Mohammad R. Alenezi. "UV Sensor Based on Single Metal Oxide Nanowire." International Journal of Engineering Sciences & Research Technology, 2014, 7, 755−758.
17. Mohammad R. Alenezi, Talal H. Alzanki, Abdullah S. Alshammari, Simon John Henley, and S. Ravi P. Silva "UV Sensing Properties of Single 2D ZnO Nanostructure." Journal of Materials Science and Engineering A 2014, 4, 197−201.
18. Mohammad R. Alenezi, Abdullah S. Alshammari, K. D. G. I. Jayawardena, Michail J Beliatis, Simon J. Henley and S. R. P. Silva. Role of the Exposed Polar Facets in the Performance of Thermally and UV Activated ZnO Nanostructured Gas Sensors. J. Phys. Chem. C, 2013, 117, 17850–17858.
19. P. Feng, Q. Wan, T.H. Wang, Contact-controlled sensing properties of flowerlike ZnO nanostructures, Appl. Phys. Lett. 87 (2005) 213111/1–213111/3.
20. C.C. Li, Z.F. Du, L.M. Li, H.C. Yu, Q. Wan, T.H. Wang, Surface-depletion controlled gas sensing of ZnO nanorods grown at room temperature, Appl. Phys. Lett. 91 (2007) 032101/1–032101/3.
21. Y. Chen, C.L. Zhu, G. Xiao, Reduced-temperature ethanol sensing characteristics of flower-like ZnO nanorods synthesized by a sonochemical method, Nanotechnology 17 (2006) 4537–4541.
22. Q. Yuan, Y.P. Zhao, L. Li, T. Wang, Ab initio study of ZnO-based gas-sensing mechanisms: surface reconstruction and charge transfer, J. Phys. Chem. C 113 (2009) 6107–6113.
23. N. Hongsith, E. Wongrat, T. Kerdcharoen, S. Choopun, Sensor response formula for sensor based on ZnO nanostructures. Sensors and Actuators B 2010, 144, 67–72.
24. Feng, P.; Xue, X. Y.; Liu, Y. G.; Wang, T. H. Highly sensitive ethanol sensors based on {100}-bounded In2O3 nanocrystals due to face contact. Appl. Phys. Lett. 2006, 89, 243514/1– 243514/3.
25. C. Ye, T. Tamagawa, D. L. Polla, Experimental studies on primary and secondary pyroelectric effects in $Pb(ZrxTi1-x)O_3$, $PbTiO_3$, and ZnO thin films. J. Appl. Phys. 1991, 70, 5538− 5543.
26. A. D. Bykhovski, V. V. Kaminski, M. S. Shur, Q. C. Chen, M. A. Khan, Pyroelectricity in gallium nitride thin films. Appl. Phys. Lett. 1996, 69, 3254−3256.
27. Y. K. Jun, H. S. Kim, J. H. Lee, S. H. Hong, CO sensing performance in micro-arc oxidized $TiO_2$ films for air quality control. Sens. Actuator B, 2006, 120, 69–73.
28. M. Kugishima, S. Sakai, K. Shimanoe, N. Yamazoe, Development of SnO2-based gas sensor sensitive to dilute ethylene oxide in air. Sens. Actuator B, 2005, 108, 130–133.
29. P. S. Cho, K. W. Kim, J. H. Lee, $NO_2$ sensing characteristics of ZnO nanorods prepared by hydrothermal method. J. Electroceram., 2006, 17, 975–978.
30. Y. Zeng, T. Zhanga, M. Yuan, M. Kang, G. Lu, R. Wang, H. Fan, Y. He, H. Yang, Growth and selective acetone detection based on ZnO nanorod arrays. Sens. Actuator B, 2009, 143, 93–98.



 